

Steady and Unsteady Buckling of Viscous Capillary Jets and Liquid Bridges

Jingxuan Tian

Department of Mechanical Engineering, The University of Hong Kong, Pokfulam Road, Hong Kong, China

Neil M. Ribe^{*}

Lab FAST, University Paris-Saclay, CNRS, Bât. 530, Campus Univ, 91400 Orsay, France

Xiaoxiao Wu[†]

Faculties of Sciences and Engineering, The University of Hong Kong, Pokfulam Road, Hong Kong, China

Ho Cheung Shum[†]

Department of Mechanical Engineering, The University of Hong Kong, Pokfulam Road, Hong Kong, China

 (Received 20 March 2020; revised 2 June 2020; accepted 23 July 2020; published 3 September 2020)

Steady buckling (coiling) of thin falling liquid jets is sensitive to surface tension, yet an understanding of these capillary effects lags far behind what is known about surface-tension-free coiling. In experiments with submillimetric jets and ultralow flow rates, we find that the critical dispensing height H_c for coiling decreases with increasing flow rate, a trend opposite to that found previously for inertia-free coiling. We resolve the apparent contradiction using nonlinear numerical simulations based on slender-jet theory which show that the trend reversal is due to the strong effect of surface tension in our experiments. We use our experiments to construct a regime diagram (coiling vs stagnation flow) in the space of capillary number Ca and jet slenderness ϵ and find that it agrees well with fully nonlinear numerical simulations. However, it differs substantially from the analogous regime diagram determined experimentally by Le Merrer, Quéré, and Clanet [*Phys. Rev. Lett.* **109**, 064502 (2012)] for the unsteady buckling of a compressed liquid bridge. Using linear stability analysis, we show that the differences between the two regime diagrams can be explained by a combination of shape nonuniformity and the influence of gravity.

DOI: [10.1103/PhysRevLett.125.104502](https://doi.org/10.1103/PhysRevLett.125.104502)

An elastic rod compressed along its axis buckles when the load exceeds a critical value, a phenomenon first studied by Euler in the 18th century. Liquid “rods” can also buckle under compression; here the resisting force is due to viscosity. A liquid bridge compressed sufficiently rapidly between rigid pistons eventually bends; this is an example of unsteady buckling [1]. By contrast, steady buckling occurs when the liquid falls continuously downward from a nozzle onto a stationary surface. This “liquid rope coiling” (LRC) has been intensively studied during the past 60 years using laboratory experiments, linear stability analysis, asymptotic analysis, and numerical simulation [2–12]. LRC is interesting not only for the rich dynamics emerging from the interplay of the multiple forces involved, but also because it is encountered in practical situations such as additive manufacturing of functional materials [13–17] and ultrafine viscous liquid dispensing [18–22]. The high resolution involved here is achieved by dispensing very thin jets at very low flow rates. The effects of surface tension should therefore be particularly strong. Yet all existing studies of LRC consider vanishing [9,11] or weak [8,23] surface tension. Understanding the coiling of capillary jets with strong surface tension is essential not only for completing

the big picture of LRC dynamics but also for a variety of applications in high-resolution extrusion-based printing and liquid dispensing.

Here we combine experiments, nonlinear numerical simulation and linear stability analysis (LSA), to reveal the dynamics of surface-tension-dominated LRC in the limit of negligible inertia. We gain further understanding by comparing steady buckling with unsteady buckling [1] using LSA. To our knowledge, ours is the first study to elucidate LRC for capillary jets using three independent approaches that agree closely with one another.

Experimental procedure.—We used silicone oils (Sigma Aldrich) with viscosities 3.2–60 Pa s measured by a rheometer (Anton Paar). The fluid was extruded from a glass syringe activated by a syringe pump fixed to an elevatable platform [Fig. 1(a)]. Figure 1(b) shows a schematic of the jet. The flow rate ranged from 1.5 to 150 mL/h. Visual data was recorded by high-speed camera (Photron).

Critical height vs flow rate.—As the fall height increases beyond a critical value H_c with the flow rate held fixed, an initially straight jet exhibits incipient buckling that quickly turns into finite-amplitude coiling [Fig. 1(c)]. A similar transition occurs as the flow rate increases for a fixed

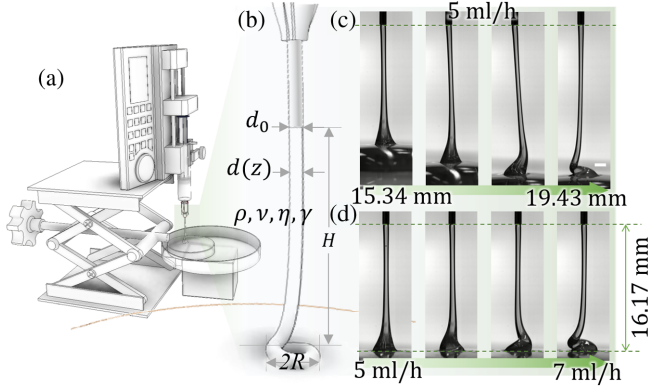


FIG. 1. (a) Experimental setup. (b) Schematic of the extruded jet with density ρ , kinematic viscosity ν , dynamic viscosity η , surface tension coefficient γ , nozzle diameter d_0 , and jet diameter $d(z)$. (c) Photographs of the jet for fixed flow rate Q and increasing fall height H , showing the transition from stagnation flow to coiling. The scale bar is 1 mm. (d) Still photographs of a similar transition at a fixed fall height with increasing flow rate.

dispensing height [Fig. 1(d)]. Figure 2 shows H_c (solid lines) as a function of flow rate Q for six sets of experiments with different viscosities. H_c decreases with Q within each set. This is opposite to the trend previously found [23,24] for surface-tension-free coiling with negligible inertia, for which H_c is either independent of flow rate (“viscous” regime) or increases with flow rate (“gravitational” regime).

One clue to the cause of this discrepancy is the scaled-down character of our experiments. Compared to previous studies [2,4,23,25], we use nozzle diameters ($d_0 = 0.6\text{--}1.55$ mm) smaller by a factor of ≈ 2 and flow rates ($Q = 1.5\text{--}150$ mL/h) smaller by ≈ 2 orders of magnitude. A comparison of parameters is found in [26], Table S1. Another clue is that our critical heights H_c are as large as $\approx 93d_0$, about 15 times the largest values $\approx 5\text{--}6d_0$ from the existing literature ([26], Table S2). Both clues suggest the hypothesis that the discrepancy is due to strong surface tension. To test this, we use a slender-jet model [9] implemented in the continuation and bifurcation software AUTO-07P [27] to simulate coiling with strong surface tension. In the limit of negligible inertia, the critical height H_c can depend only on d_0 , Q , ν , ρg , and γ . The Π -theorem of dimensional analysis then implies that three independent dimensionless groups can be formed from these six parameters. We choose these groups to be

$$\frac{H_c}{d_0}, \quad \left(\frac{\nu Q}{gd_0^4}\right)^{1/4} \equiv \Pi_Q, \quad \frac{\rho g d_0^2}{\gamma} \equiv Bo, \quad (1)$$

where Π_Q is a dimensionless flow rate and the Bond number Bo is the ratio of gravitational to capillary forces. Following [28], we define H_c as the height at which the numerically predicted radius a_1 of the lowermost part of the coiling jet just equals the radius R of the coil itself

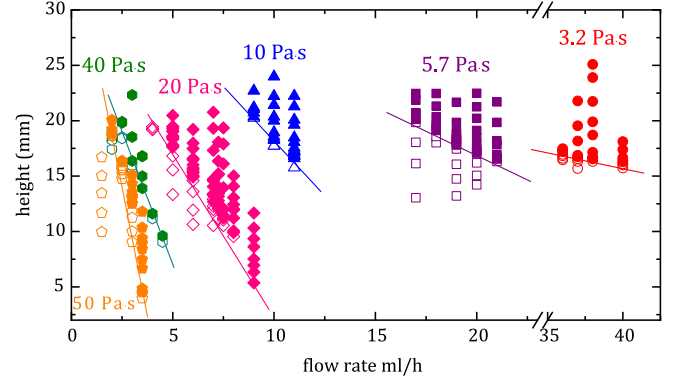


FIG. 2. Experimentally determined critical height for the onset of coiling as a function of flow rate and viscosity. The needle diameter is $d_0 = 0.6$ mm. Different colors correspond to different viscosities as indicated. Solid symbols represent coiling, whereas open symbols correspond to stagnation flow. Solid lines are drawn by eye to fit the boundaries between open and solid symbols to indicate a decreasing trend.

because $a_1 > R$ corresponds to unphysical self-penetration. Figure 3 shows our calculated critical heights (solid lines) together with our experimental measurements (symbols) as functions of Π_Q for several values of Bo . Despite a small

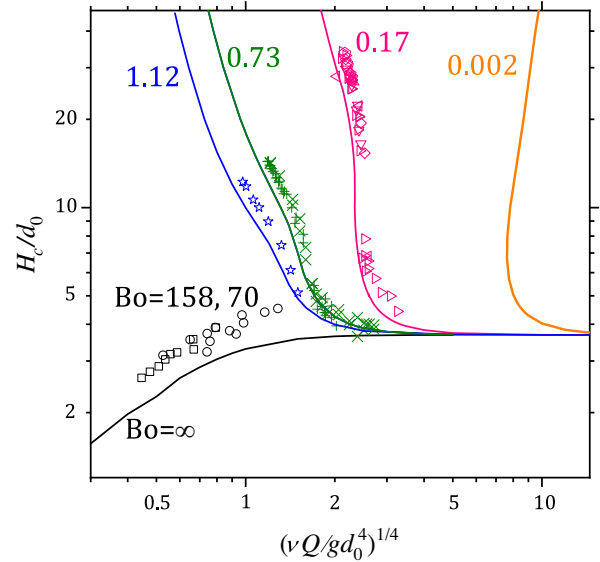


FIG. 3. Numerically predicted (lines) and experimentally measured (symbols) critical heights H_c vs Π_Q for several values of the Bond number Bo ([26], Note S4). The black line replicates a previous result for $Bo = \infty$ [28] and is compared to experimental data of [4] for $Bo = 158$ (squares) and 70 (circles). The other four curves are for the values of Bo indicated. The symbols represent different viscosities: 3.2 Pas (up-pointing triangles), 5.7 Pas (pentagons), 10 Pas (right-pointing triangles, stars, and + symbol), 20 Pas (down-pointing triangles), 30 Pas (x symbol), 40 Pas (diamonds), and 50 Pas (left-pointing triangles). The corresponding onset frequencies (both measured and predicted) are shown in [26], Fig. S1.

systematic offset, the measured data points and the calculated curves track each other well. For large $Bo \geq 70$ (negligible surface tension), H_c increases with the flow rate, whereas it decreases when $Bo \leq 1.12$ (strong surface tension). This is the apparent contradiction that we pointed out earlier between the results of this study and those of [4,5,23]; we now see that it is due to the large effect of surface tension in our experiments.

Regime diagram for buckling.—Steady buckling (LRC) is induced by injecting fluid into the upper end of a jet while keeping the fall height fixed. By contrast, in unsteady buckling, the height of a compressed liquid bridge decreases while the deflection of the centerline increases monotonically. Yet while steady and unsteady buckling show these obvious differences, a deeper physical understanding of both can be obtained by comparing them. To do this we construct a regime diagram (LRC vs stagnation flow) in the space of jet slenderness $d_0/H \equiv \epsilon$ and capillary number $\eta U_0/\gamma \equiv Ca$, following the procedure used by [1] for unsteady buckling. Here $U_0 = 4Q/\pi d_0^2$ is the mean extrusion velocity, and $Ca = (4/\pi)\Pi_Q^4 Bo$. Figure 4 shows our experimental data for steady buckling in the ϵ - Ca plane, together with the critical curve (black dashed line) for unsteady buckling of [1]. One sees immediately that the domain of steady buckling (filled symbols) is larger than that of unsteady buckling, extending both to lower values of $Ca < 8.5$ and to higher values of $\epsilon > 0.1$.

Also shown in Fig. 4 are critical curves for steady buckling calculated numerically for three values of Bo . $Bo = 0.73$ corresponds to the experimental data shown in green and yellow, while $Bo = 0.17$ corresponds to pink and violet data. The good agreement of the calculated critical curves with the experimentally observed regime boundaries shows that the minimum value of Ca for which buckling occurs depends strongly on Bo , i.e., on the effect of gravity relative to surface tension. Gravity is relatively unimportant in the upper part of the diagram where the three critical curves coincide.

Linear stability analysis.—We now turn to LSA, which unlike the nonlinear slender-jet model can be applied to both steady (jet) and unsteady (bridge) buckling, allowing us to compare them consistently. The analysis will elucidate the distinct causes of the greater rightward (to larger ϵ) and downward (to smaller Ca) extents of the steady buckling region relative to the unsteady buckling region in Fig. 4. We first demonstrate the relevance of LSA by using it to predict accurately the critical buckling height and frequency for one of our experiments on LRC ([26], Note S1). Now we apply LSA to unsteady buckling of a compressed liquid bridge.

Without loss of generality, we suppose that buckling is confined to the $x_1 - x_3$ plane, where $x_3 \equiv z$ increases downward. We further suppose that the lateral deflection ζ of the jet's axis is small. In the absence of inertia, the

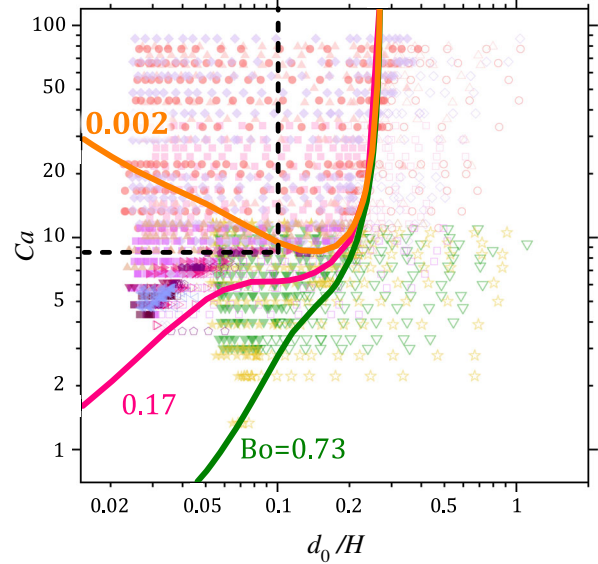


FIG. 4. Regime diagram for steady buckling (LRC) in the space of jet slenderness $d_0/H \equiv \epsilon$ and capillary number $\eta U_0/\gamma \equiv Ca$. Solid lines indicate the stagnation to coiling transition predicted by nonlinear numerical simulations of LRC for $Bo = 0.73, 0.17$, and 0.002 . The dashed black line is the critical curve for unsteady buckling [1]. Experimental data are indicated by filled symbols (coiling) and open symbols (stagnation flow). The pink and violet symbols are for $Bo = 0.17$, and the yellow and green symbols are for $Bo = 0.73$. Viscosities used are 3.2 Pa s (deep plum downward-pointing triangles), 5.7 Pa s (orchid left-pointing triangles), 10 Pa s (light pink squares), 20 Pa s (deep pink right-pointing triangles), 23 Pa s (blush pink circles), 30 Pa s (light brown triangles), 40 Pa s (light violet diamonds), and 50 Pa s (purple pentagons) for $Bo = 0.17$; 10 Pa s (yellow stars) and 30 Pa s (green downward-pointing triangles) for $Bo = 0.73$. Analogous results for $Bo = 0.032$, which like the case $Bo = 0.002$ exhibits multiple onset heights, can be found in [26], Note S5, and the supplemental video.

equations of force balance perpendicular to and parallel to the jet's axis are [10]

$$-M_2'' + \kappa_2 N_3 + \frac{\pi}{2} \gamma d \kappa_2 - \rho A g \zeta' = 0, \quad (2a)$$

$$N_3' + \frac{\pi}{2} \gamma d' + \rho A g = 0, \quad (2b)$$

where $N_3(z)$ is the normal viscous force on the cross section, $M_2(z, t)$ is the bending moment, $A = \pi d^2/4$, $\kappa_2 \equiv \zeta''(z, t)$ is the curvature of the axis about the x_2 direction, and primes denote $\partial/\partial z$. The constitutive relations for N_3 and M_2 are $N_3 = 3\eta A U_3'$ and $M_2 = 3\eta I(\zeta'' + U_3 \zeta'''' - U_3' \zeta''/2)$ [12], where $I = \pi d^4/64$, U_3 is the vertical velocity on the jet's axis, and a dot indicates $\partial/\partial t$.

We now combine the foregoing equations and set $\zeta = F(z) \exp \sigma t$, where σ is the growth rate. The resulting equations for U_3 and F are

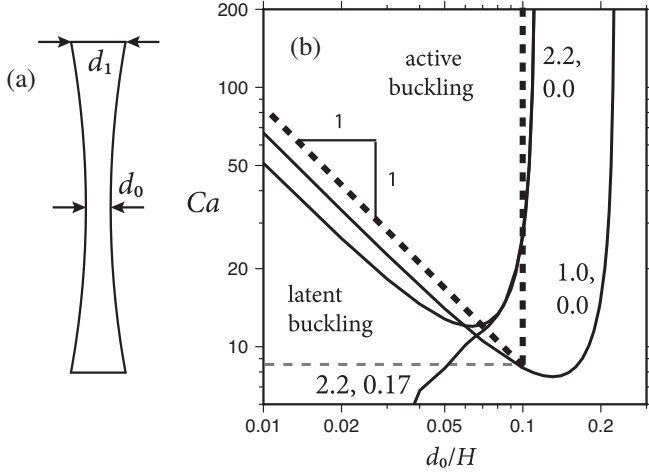


FIG. 5. Results of linear stability analysis of unsteady basic states of a compressed liquid bridge. (a) Prescribed parabolic shape of the bridge for $d_1/d_0 = 2.2$. (b) Critical curves for unsteady buckling in the d_0/H - Ca space. The three solid curves are predicted by linear stability analysis for the values of $(d_1/d_0, Bo)$ indicated. The dashed lines bound the regions of active and latent unsteady buckling of [1].

$$3\eta(d^2U_3')' + 2\gamma d' + \rho g d^2 = 0, \quad (3a)$$

$$\left[d^4 \left(\sigma F'' + U_3 F''' - \frac{1}{2} U_3' F'' \right) \right]'' - 16 \left(d^2 U_3' + \frac{2\gamma}{3\eta} d \right) F'' + \frac{16\rho g}{3\eta} d^2 F' = 0. \quad (3b)$$

Equation (3b) together with the “clamped” boundary conditions $F(0) = F'(0) = F''(0) = F(H) = F'(H) = 0$ is an eigenvalue problem for $F(z)$ that can be solved if $d(z)$ and $U_3(z)$ are known. A critical difference between a clamped liquid bridge and a flowing jet is that the diameter $d(z)$ is highly nonuniform in the former case. To approximate the shape of a static liquid bridge before it is compressed, we assume $d = d_0 + (d_1 - d_0)(2z - H)^2/H^2$, where d_0 is the diameter in the center and d_1 the diameter at either end. Figure 5(a) shows this shape for $d_1/d_0 = 2.2$, a value determined by least-squares fitting of the assumed quadratic shape to the central 50% of the bridge shown in the leftmost image of Fig. 1(a) of [1]. The known function $d(z)$ is now injected into Eq. (3) with $g = 0$, which can then be solved analytically subject to $U_3(0) = U_0$ and $U_3(H) = 0$ ([26], Note S2). The eigenvalue problem for $F(z)$ is then solved using AUTO-07P. The only eigenvalues are two positive real ones, which lie on a double-valued (folded) surface above the ϵ - Ca plane. These correspond to amplified buckling without oscillation, as observed by [1]. To determine where in the ϵ - Ca plane such growing modes exist, we start from either mode and continue it to higher ϵ and/or lower Ca until a turning point is encountered beyond which the solution no longer exists. The locus of all such turning points is a critical

curve that divides the ϵ - Ca plane into two regions where buckling occurs and does not occur.

Figure 5(b) shows those critical curves (solid lines) for three combinations of values of d_1/d_0 and Bo . The dashed lines bound the regions of active and latent unsteady buckling proposed by [1] ([26], Note S3) such that bridges initially in the latent region remain straight while their slenderness ϵ increases until they reach the active region. The “reference” critical curve for $(d_1/d_0, Bo) = (2.2, 0.0)$ agrees well with the boundaries of the active buckling region of [1]. Relative to this, the curve with $(d_1/d_0, Bo) = (1.0, 0.0)$ shows that buckling of a uniform bridge occurs for values of the slenderness ϵ that are about twice as great as those for a nonuniform bridge with $d_1/d_0 = 2.2$. This is because the thicker ends of the nonuniform bridge resist buckling more effectively than the thinner ends of the uniform bridge. In summary, the maximum slenderness d_0/H for which unsteady buckling occurs depends strongly on the shape of the bridge.

Continuing with Fig. 5(b), we explore the effect of gravity by comparing the reference curve with the curve for $d_1/d_0 = 2.2$ and $Bo = 0.17$, the values in the experiments of [1]. Whereas the two curves coincide for $Ca > 12$, they are quite different for lower values of Ca and even the signs of their slopes are opposite. Active unsteady buckling should occur everywhere above and to the left of the curve with $Bo = 0.17$. However, this is not what was seen in the experiments of [1], who observed buckling only above a horizontal line $Ca = 8.5$. The reason for this disagreement between experiment and theory is unclear.

Discussion.—This work began as an effort to understand why the critical height for steady buckling of capillary jets decreases as a function of flow rate, a trend opposite to that seen in previous studies of inertia-free coiling. The small nozzle sizes and flow rates used in our experiments, as well as our observations of unusually long stable jets, suggested that the trend reversal was due to strong surface tension, a hypothesis that we confirmed with fully nonlinear slender-jet numerical simulations. The importance of surface tension relative to viscous forces in steady buckling can also be estimated roughly as the characteristic ratio of the surface tension force $F_\gamma \sim \gamma a_1 R^{-1}$ to the viscous force $F_v \sim \rho v a_1^4 U_0 R^{-4}$, where R is the coil radius, a_1 is the radius of the jet within the coil, and $U_1 \equiv Q/\pi a_1^2$ is the axial velocity of the fluid in the coil [9]. We find that $F_\gamma/F_v = 1.1$ – 2.3 for our experiments, indicating the crucial importance of surface tension.

We gained further physical insight by comparing our experimental phase diagram for steady buckling in the ϵ - Ca plane with an analogous diagram for unsteady buckling [1]. There are two major differences between the two diagrams. First, steady buckling occurs up to $\epsilon \approx 0.25$, greater than the maximum slenderness $\epsilon \approx 0.1$ for unsteady buckling. Second, steady buckling occurs for capillary numbers as low as 1.3, whereas unsteady buckling is limited to $Ca \geq 8.5$. These two differences have distinct causes that we were able to elucidate using

finite-amplitude numerical simulation and linear stability analysis. The different ranges of ϵ are explained by a difference in shape of the buckling object: a steadily coiling capillary jet has a nearly constant diameter, whereas a buckling liquid bridge has strongly thickened ends that oppose a greater resistance to bending. The cause of the different ranges of Ca is more subtle. First, note that all three of our independent approaches (experiments for steady buckling, numerical simulation of steady coiling, and LSA of unsteady buckling) agree in showing that the minimum value of Ca for buckling decreases as gravity becomes more important relative to surface tension, i.e., as Bo increases. This result would explain the difference between our regime diagram and that of [1] if gravity were negligible in the latter study. This is not so, however, because $Bo = 0.17$ in the experiments of [1]. According to our LSA, a gravitational effect of this magnitude relative to surface tension should permit unsteady buckling to occur well below the lower limit $Ca = 8.5$ observed by [1]. Further analysis and experiments are needed to resolve this contradiction.

Our work has important applications to microscale manipulation of viscous fluid threads in situations such as high-resolution printing of intricate patterns and functional architectures. The current trend toward ever smaller scales means that surface tension will play a crucial role in future applications. The present work may therefore provide timely guidance for practice. On the theoretical side, asymptotic analysis similar to that of [3] could help to elucidate the detailed mechanism by which strong surface tension reverses the trend of the variation of onset height as a function of flow rate. In closing, we note that our investigation of the effects of surface tension has been limited to coiling in the inertia-free viscous and gravitational regimes. Future research on the influence of surface tension on inertial coiling will bring us closer to a complete physical picture of liquid rope coiling.

This work was supported by the General Research Fund (Nos. 17306315 and 17329516) and the Research Impact Fund (R7072-18) of the University of Hong Kong, the NSFC Excellent Young Scientists Fund (Hong Kong and Macau) (21922816) and by the PROCORE France/Hong Kong Joint Research Scheme (Nos. 40424RF and F-HKU703/17) from the Partenariat Hubert Curien and the Research Grants Council of Hong Kong. The authors thank the anonymous referees for their helpful comments.

J. T. and N. M. R. contributed equally to this work.

*Corresponding author.
ribe@fast.u-psud.fr

†Corresponding author.
ashum@hku.hk

- [1] M. Le Merrer, D. Quéré, and C. Clanet, Buckling of Viscous Filaments of a Fluid Under Compression Stress, *Phys. Rev. Lett.* **109**, 064502 (2012).
- [2] G. Barnes and R. Woodcock, Liquid rope-coil effect, *Am. J. Phys.* **26**, 205 (1958).
- [3] M. J. Blount, Bending and buckling of a falling viscous thread, Ph.D. Thesis, University of Cambridge, 2010, <https://www.repository.cam.ac.uk/handle/1810/252208>.
- [4] J. O. Cruickshank, Viscous fluid buckling: A theoretical and experimental analysis with extensions to general fluid stability, Ph.D. Thesis, Iowa State University, 1980, <https://lib.dr.iastate.edu/rtd/6692/>.
- [5] J. O. Cruickshank and B. R. Munson, Viscous fluid buckling of plane and axisymmetric jets, *J. Fluid Mech.* **113**, 221 (1981).
- [6] M. Habibi, M. Maleki, R. Golestanian, N. M. Ribe, and D. Bonn, Dynamics of liquid rope coiling, *Phys. Rev. E* **74**, 066306 (2006).
- [7] L. Mahadevan, W. S. Ryu, and A. D. T. Samuel, Correction: Fluid 'rope trick' investigated, *Nature (London)* **403**, 502 (2000).
- [8] M. Maleki, M. Habibi, R. Golestanian, N. M. Ribe, and D. Bonn, Liquid Rope Coiling on a Solid Surface, *Phys. Rev. Lett.* **93**, 214502 (2004).
- [9] N. M. Ribe, Coiling of viscous jets, *Proc. R. Soc. A* **460**, 3223 (2004).
- [10] N. M. Ribe, M. Habibi, and D. Bonn, Stability of liquid rope coiling, *Phys. Fluids* **18**, 084102 (2006).
- [11] N. M. Ribe, H. E. Huppert, M. A. Hallworth, M. Habibi, and D. Bonn, Multiple coexisting states of liquid rope coiling, *J. Fluid Mech.* **555**, 275 (2006).
- [12] B. Tchavdarov, A. L. Yarin, and S. Radev, Buckling of thin liquid jets, *J. Fluid Mech.* **253**, 593 (1993).
- [13] H.-Y. Kim, M. Lee, K. J. Park, S. Kim, and L. Mahadevan, Nanopottery: Coiling of electrospun polymer nanofibers, *Nano Lett.* **10**, 2138 (2010).
- [14] J. Li, T. Kong, J. Yu, K. H. Lee, Y. H. Tang, K. Kwok, J. T. Kim, and H. C. Shum, Electrocoiling-guided printing of multiscale architectures at single-wavelength resolution, *Lab Chip* **19**, 1953 (2019).
- [15] J. I. Lipton and H. Lipson, 3d printing variable stiffness foams using viscous thread instability, *Sci. Rep.* **6**, 29996 (2016).
- [16] R. Passieux, L. Guthrie, S. H. Rad, M. Lévesque, D. Therriault, and F. P. Gosselin, Instability-assisted direct writing of microstructured fibers featuring sacrificial bonds, *Adv. Mater.* **27**, 3676 (2015).
- [17] H. Yuk and X. Zhao, A new 3d printing strategy by harnessing deformation, instability, and fracture of viscoelastic inks, *Adv. Mater.* **30**, 1704028 (2018).
- [18] T. Cubaud, B. Jose, and S. Darvishi, Folded micro-threads: Role of viscosity and interfacial tension, *Phys. Fluids* **23**, 042002 (2011).
- [19] T. Cubaud and T. G. Mason, Folding of Viscous Threads in Diverging Microchannels, *Phys. Rev. Lett.* **96**, 114501 (2006).
- [20] S. Darvishi and T. Cubaud, Formation of capillary structures with highly viscous fluids in plane microchannels, *Soft Matter* **8**, 10658 (2012).

- [21] T. Kong, J. Li, Z. Liu, Z. Zhou, P. H. Y. Ng, L. Wang, and H. C. Shum, Rapid mixing of viscous liquids by electrical coiling, *Sci. Rep.* **6**, 19606 (2016).
- [22] J. Tian, J. Li, A. Sauret, T. Kong, X. Wu, Y. Lu, and H. C. Shum, Facile control of liquid-rope coiling with tunable electric field configuration, *Phys. Rev. Applied* **12**, 014034 (2019).
- [23] M. Habibi, Y. Rahmani, D. Bonn, and N. M. Ribe, Buckling of Liquid Columns, *Phys. Rev. Lett.* **104**, 074301 (2010).
- [24] N. M. Ribe, M. Habibi, and D. Bonn, Liquid rope coiling, *Annu. Rev. Fluid Mech.* **44**, 249 (2012).
- [25] M. Habibi, S. H. Hosseini, M. H. Khatami, and N. M. Ribe, Liquid supercoiling, *Phys. Fluids* **26**, 024101 (2014).
- [26] See Supplemental Material at <http://link.aps.org/supplemental/10.1103/PhysRevLett.125.104502> for (1) Fig. S1 for coiling onset frequency as a function of dimensionless flow rate, (2) note S1 for a linear stability analysis of steady buckling, (3) note S2 for the axial velocity in a compressed liquid bridge, (4) note S3 for a comparison of active and latent unsteady buckling, (5) note S4 for the sources of experimental error, (6) note S5 for the experimental observations for $Bo = 0.032$, (7) Table S1 for a comparison of parameters with those in the literature, and (8) Table S2 for the jet slenderness just before coiling onset.
- [27] E. J. Doedel, A. R. Champneys, T. F. Fairgrieve, Yu. A. Kuznetsov, B. Sandstede, and X. Wang, AUTO97 : Continuation and bifurcation software for ordinary differential equations, Department of Computer Science, Concordia University, Technical Report, 1997, <http://indy.cs.concordia.ca/auto/>.
- [28] N. M. Ribe, Liquid rope coiling: A synoptic view, *J. Fluid Mech.* **812**, R2 (2017).